Application of wavy geometries for reducing trailing edge instability noise

Tom A. Smith[1]
Dept. Mechanical Engineering, University College London
Gower Street, London, WC1E 7JE, United Kingdom

Yiannis Ventikos[2]
Dept. Mechanical Engineering, University College London
Gower Street, London, WC1E 7JE, United Kingdom

ABSTRACT

Trailing edge noise from lifting surfaces occurs across a wide range of applications, and there is a clear desire to reduce it. At moderate Reynolds numbers, high amplitude instability noise can occur where instability waves in the boundary layer are amplified close to the trailing edge before they scatter as acoustic waves. In this work, aero-acoustic simulations are conducted to demonstrate how wavy wings can be used to reduce trailing edge noise at moderate Reynolds numbers. The simulations are conducted using a hybrid aero-acoustic model, where large eddy simulations are used to compute the acoustic source terms for the acoustic perturbation equations. Wavy wings with different wavelengths are considered to understand how this affects the sound levels. The results show that modest reductions of 4 dB are achieved for wings with a spanwise sinusoidal variation but a substantial reduction of nearly 18 dB is achieved for a wing with a more random spanwise variation. It is further shown that the wavy wings can reduce the drag compared to a smooth wing for the operating condition considered. These preliminary results show that a wavy wing has substantial potential to reduce noise and drag and this warrants further investigation.

1. INTRODUCTION

Trailing edge instability noise commonly occurs for wings and other lifting bodies operating at moderate Reynolds numbers, when the boundary layer on at least one side is transitional. In the presence of a small separated region immediately upstream of the trailing edge, Tollmien-Schlichting (T-S) instability waves in the boundary layer can be amplified, before scattering as acoustic waves of the same frequency. The phenomenon has been studied for many decades, and a wealth of research can be found on the underlying physical mechanisms, as well as methods for predicting the frequencies of the noise based on analytical or semi-empirical methods [1–6].

---

[1]tom.smith.17@ucl.ac.uk

[2]y.ventikos@ucl.ac.uk

Due to the high amplitude of this type of noise and its prevalence in a number of practical applications including wind turbine blades, numerous efforts have been made to reduce it. Serrated edges [7–10], porous edges and surfaces [11–13], and also surface ridges [14] have been considered. Serrated edges work by breaking up the coherent tubular vortices associated with the T-S waves, thus reducing the spanwise correlation. Furthermore, they can act to prevent or reduce the separated region upstream of the trailing edge. Porous edges and surfaces can also act to reduce the correlation of a transitional or turbulent boundary layer, as well as reducing the convection velocity inside the boundary layer. Inspired by natural geometries, a wing with surface ridges and trailing edge serrations [14] was found to produce significantly less noise than a smooth wing, but with a small increase in the drag. This represents a challenge when trying to reduce noise, as many techniques to reduce instability noise will increase the drag. Indeed, one of the easiest ways to remove instability noise is to force the boundary layer to transition to turbulence before it reaches the trailing edge. This has been shown to be highly effective at reducing the sound pressure level, but it reduces the wing performance by increasing the drag [15].

Therefore, there is a desire to develop geometries that have a superior acoustic performance but without an increase in drag. To this end, a wavy wing has a number of potential benefits. Firstly, it can reduce the spanwise correlation of the flow as shown by [14], thus reducing the trailing edge noise. Secondly, if leading edge noise is present, there is the potential for the wavy surface to reduce the noise produced by turbulence scattering at the leading edge, as demonstrated by [16, 17]. Riblets and grooves inspired by shark skin have been used to reduce drag from turbulent boundary layers [18] and these share similarities with surface waves. It therefore seems possible that a wing incorporating surface waves or riblets might be developed that exhibits a superior acoustic characteristics without any degradation in performance in terms of lift and drag. Such a geometry could be used in a wide range of applications, including wind turbines, marine propellers, and other areas where lifting body noise is problematic.

In this work, a hybrid aero-acoustic model [19] is used to investigate the trailing edge noise produced by a series of wavy wings at a Reynolds number of Re = 64000 and an angle of attack of $\alpha = 1°$. Large eddy simulations are coupled with the acoustic perturbation equations to obtain the far-field acoustic pressure resulting from the flow over each wing. Alongside the standard NACA0012 wing, four variants are considered which have spanwise sinusoidal variations. The first three variants have a spanwise wave with a single frequency whereas the fourth has a wave consisting of the sum of two sine waves to create a more random variation in the surface geometry. The heights of the surface waves are small relative to the geometry, at 4% of the maximum wing thickness. This is to investigate whether or not a spanwise variation can be effective at reducing the noise without inducing a premature transition of the boundary layer. Whilst this would reduce the noise due to turbulent boundary layers being less efficient acoustic sources than transitional ones [20], it would also lead to a sharp increase in drag.

Validation of the overall method, as well as for the far-field noise for the smooth foil at $Re = 64000$ can be found in [19].

2. METHODS

2.1. Governing equations and numerical methods

In this study, a hybrid computational aeroacoustic code is used [19]. Incompressible large eddy simulations are first solved in the fluid domain, from which acoustic source terms are computed and then interpolated onto a larger acoustic domain. The acoustic perturbation equations are then solved in the acoustic domain to obtain the three-dimensional acoustic pressure field.

The governing equations for the fluid fields are given in equations 1 and 2.

$$\frac{\partial \hat{U}_i}{\partial x_i} = 0 \tag{1}$$

$$\frac{\partial \hat{U}_j}{\partial t} + U_j \frac{\partial \hat{U}_i}{\partial x_i} = -\frac{1}{\rho}\frac{\partial \hat{p}}{\partial x_j} + \nu \frac{\partial^2 \hat{U}_j}{\partial x_i \partial x_i} - \frac{\partial \tau_{ij}}{\partial x_i} \tag{2}$$

where

$$\tau_{ij} = \widehat{U_i U_j} - \hat{U}_i \hat{U}_j \tag{3}$$

The hat notation is used here to denote spatially filtered variables. The sub-filter scales are modelled using the Dynamic k model [21], which has been shown to be suitable for modelling transitional flows over wings [22, 23]. The equations are solved using the finite-volume approach, with a blended scheme being used to discretise the convective terms. The scheme is 75% central differencing, 25% linear upwind, which was found in [22] to be more stable than a pure central differencing scheme whilst only introducing a very small amount of dissipation into the solution. The time derivatives are discretised using a three-point backward scheme.

The acoustic source terms, defined in equation 4, are interpolated from the fluid domain to the acoustic domain using radial basis function (RBF) interpolation.

$$S = -\frac{\partial \hat{p}}{\partial t} - \hat{U}_i \frac{\partial \hat{p}}{\partial x_i} \tag{4}$$

This method interpolates the source terms to each acoustic cell using a cloud of points from the fluid domain that are close to the location of the acoustic cell. For a typical hexahedral mesh in three dimensions, 25 fluid cells are used for each interpolation. Using a scale-invariant multi-quadric basis function, this method is very accurate and robust. Details of the method, together with accuracy and convergence characteristics can be found in [19].

The acoustic perturbation equations (equations 5 and 6) are a system of four hyperbolic equations for the acoustic pressure (p_a) and velocity (U_{a_i}).

$$\frac{\partial p_a}{\partial t} + \bar{U}_i \frac{\partial p_a}{\partial x_i} + \rho_0 c_0^2 \frac{\partial u_{a_i}}{\partial x_i} = S \tag{5}$$

$$\frac{\partial u_{a_j}}{\partial t} + \bar{U}_i \frac{\partial u_{a_i}}{\partial x_j} + \frac{1}{\rho_0}\frac{\partial p_a}{\partial x_j} = \mathbf{0} \tag{6}$$

Here, $\bar{U}_i$ denotes the mean fluid velocity, c_0 and ρ_0 denote the speed of sound and fluid density respectively and are assumed to be spatially invariant. As with the fluid equations, the acoustic perturbation equations are solved using the finite volume framework. The flux evaluation is done using an exact Riemann solver with linear reconstruction, which ensures conservation and can be applied to unstructured grids with no restriction on cell type. The spatial discretisation reduces the equations to a system of ordinary differential equations, which are solved using a third-order strong stability preserving Runge-Kutta scheme.

For a typical low Mach number problem, the time-step for the acoustic solver will be smaller than for the fluid solver. For the cases considered here, $M_a = 0.023$ which requires 30 acoustic time-steps per fluid timestep. The Courant number for both parts of the simulation is $C < 1.0$.

The method is implemented within OpenFOAM. Both parts are solved simultaneously and in parallel which reduces the computational time and memory requirements.
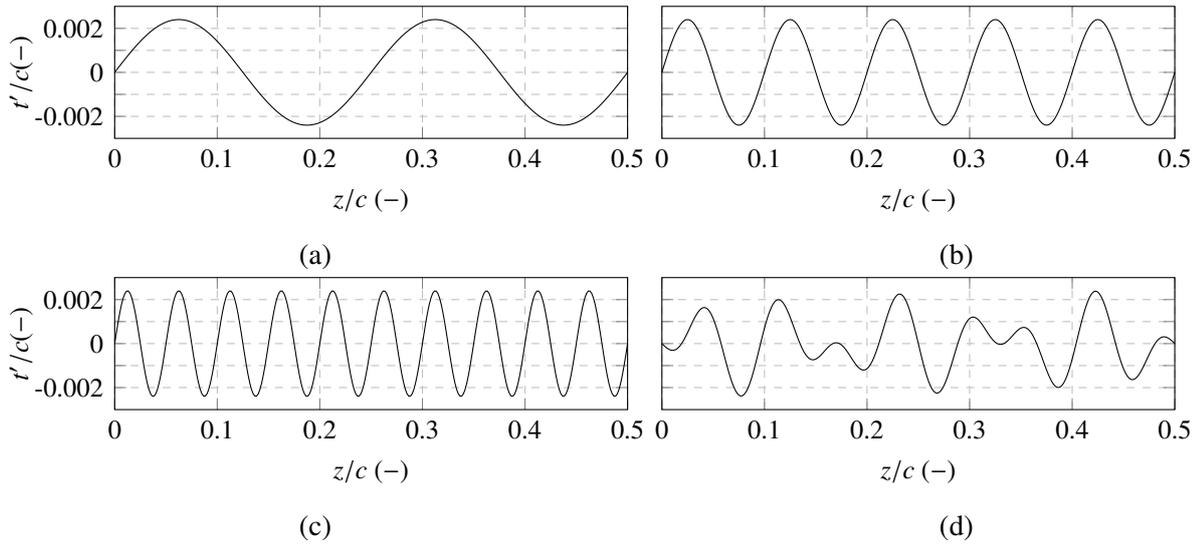
Figure 1: Spanwise surface variation for (a) variant 1, (b) variant 2, (c) variant 3, and (d) variant 4.

2.2. Geometry and meshing

The wing geometries used in this study are based on the NACA0012 airfoil. Each wing has a chord length of $c = 0.12$m and a span of $s = 0.06$m. Alongside a wing with the usual NACA0012 profile, 4 variations are considered which have a spanwise wavy surface. The wavy geometry is uniform along the chord length, and is designed such that the mean thickness of the foil remains the same as the original NACA0012 wing. The wavy surface for the first three variants consists of a single sine wave with a height of $h = 0.04t/c$ and wavelengths of $\lambda/c = 0.25, 0.1, 0.05$ respectively. The fourth variant has a surface modified by adding two waves together with heights of $h = 0.02t/c$ and wavelengths of $\lambda/c = 0.1, 0.0625$. These wavelengths were chosen to create a more irregular surface variation while maintaining spanwise periodicity. The spanwise variation in thickness for each variant relative to the smooth NACA0012 wing is shown in figure 1.

A dual-domain approach is used with the hybrid model with partially overlapping grids. This is illustrated in figure 2. The fluid domain extends three chord-lengths upstream of the wing and ten lengths downstream. The wing is pinned at either side by periodic boundaries. The fluid mesh is block-structured and consists of hexahedral cells. The resolution is based on the sensitivity studies carried out in [22] with an additional level of spanwise refinement to ensure that the three dimensional flow resulting from the surface geometry is adequately resolved. The non-dimensional near-wall grid resolution satisfies $\zeta^+ < 10$, $\eta^+ < 1$, and $z^+ < 12$ where ζ, η, z denote the chordwise, wall-normal, and spanwise directions respectively.

The acoustic domain is designed to allow for the acoustic waves to propagate spherically and so the wing is not pinned at the sides but is located in the middle of a 4m × 4m × 4m domain. The acoustic mesh is hex-dominant and is refined in the acoustic source region around the foil and also up to 1.5m away from the wing in all directions to allow for the waves to propagate without artificial dissipation. Verification studies presented in [19] showed that around 30 cells per wavelength is needed for this, and the grid used has a resolution of 0.01m. This means that acoustic waves with frequencies up to 1150Hz should be fully resolved. The experimental data [6] against which simulations of the smooth wing were compared in [19] showed that the dominant frequency was approximately 300Hz. The mesh is coarsened towards the far-field boundaries, and a perfectly matched layer is used to attenuate the waves close to the boundaries and prevent unwanted wave reflections.
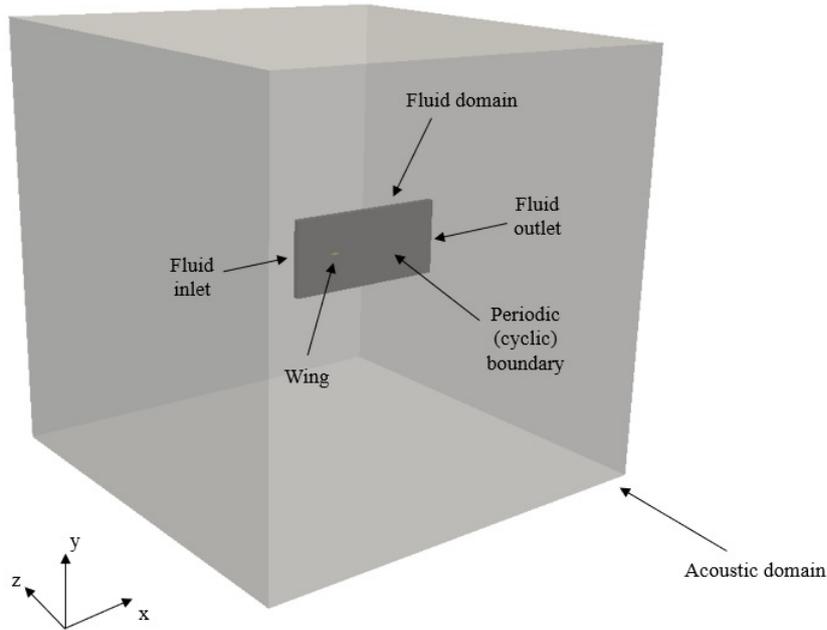
Figure 2: Illustration of the dual-domains used for the simulation

3. RESULTS

Each simulation has been run for 20 chord-flow times. The sound pressure levels have been computed using data from the last 8 chord-flow times, which is split into two windows with a 50% overlap. A reference pressure of $p_{ref} = 20\mu$Pa is used to compute the sound pressure levels. The surface pressure fluctuations are presented in the form of pressure coefficients, where $C_p = p/0.5\rho U_\infty^2$.

Figure 3 shows the overall sound pressure level 1.5m from the wing at mid span for each case. This figure shows the expected dipole pattern for each case, with the maximum sound pressure level being just less than 40 dB at $\theta = 90°$ for the smooth wing. The first three variants show similar results, with a modest reduction of approximately 4 dB when compared to the smooth wing at $\theta = 90°$. The fourth variant shows a far more significant reduction of almost 18 dB compared to the smooth wing, with a large reduction being seen at all angles.

Further insight can be gained by looking at the frequency content of the noise for each case in figure 4. The noise from the smooth foil is dominated by a single narrowband component associated with the T-S instability waves in the boundary layer. There are commonalities in the spectral content of the first three variants. Firstly, all are still dominated a narrowband component centred around 300 Hz, which is the same as the frequency of the T-S waves. In all three cases, the peak is lower than for the smooth wing. However, with reducing surface wavelength, there is an increase in higher frequency noise, particularly for variant 3, which does have a marginally higher overall SPL than variants 1 and 2. For the fourth variant, the sound levels are lower across the frequency range. The 300 Hz component is still present and there is also a tonal component at 430 Hz, but the overall signature is more broadband, suggesting that the surface waves have significantly modified the dynamics of the boundary layer transition process.

To help understand the changes in the sound levels, figure 5 shows iso-Q contours for each case to illustrate the nature of the boundary layer. For the smooth wing, tubular vortices can be seen upstream of the trailing edge which have a very strong spanwise coherence. This behaviour
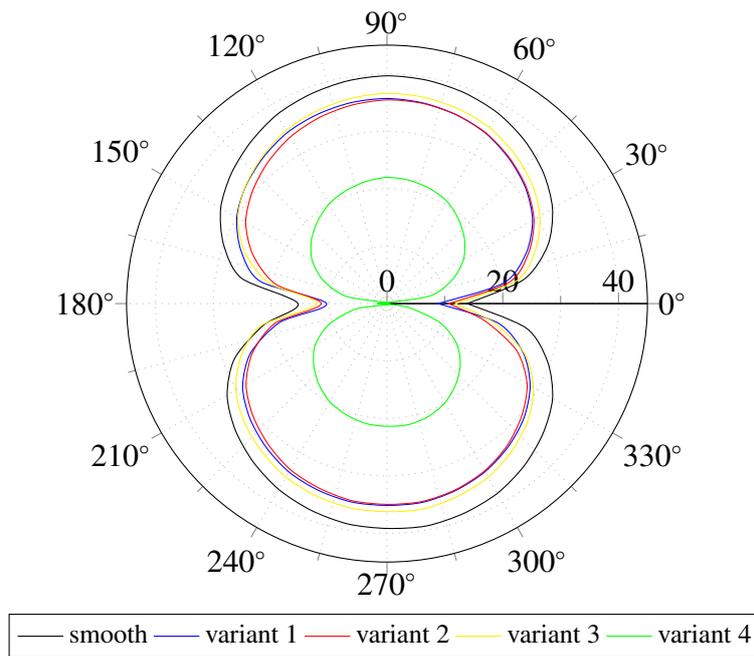
Figure 3: Directivity plot of the overall sound pressure level for the smooth wing and 4 wavy wings at 1.5m from the wing and at midspan. The reference pressure is $p_{ref} = 20\mu Pa$
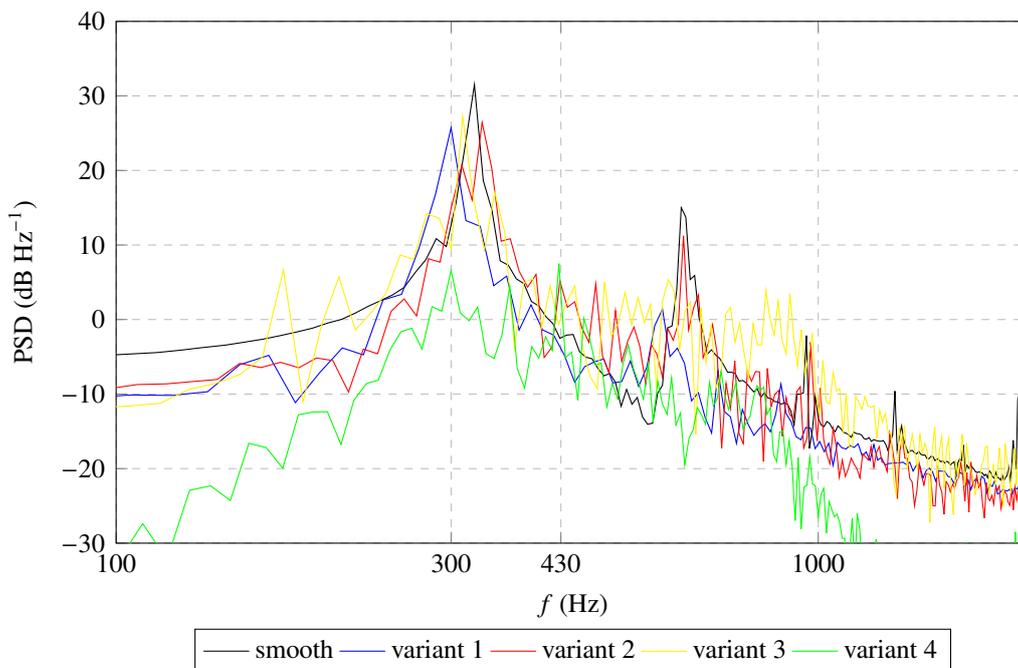

Figure 4: Sound pressure level at $\theta = 90°$ for smooth wing and 4 variants.
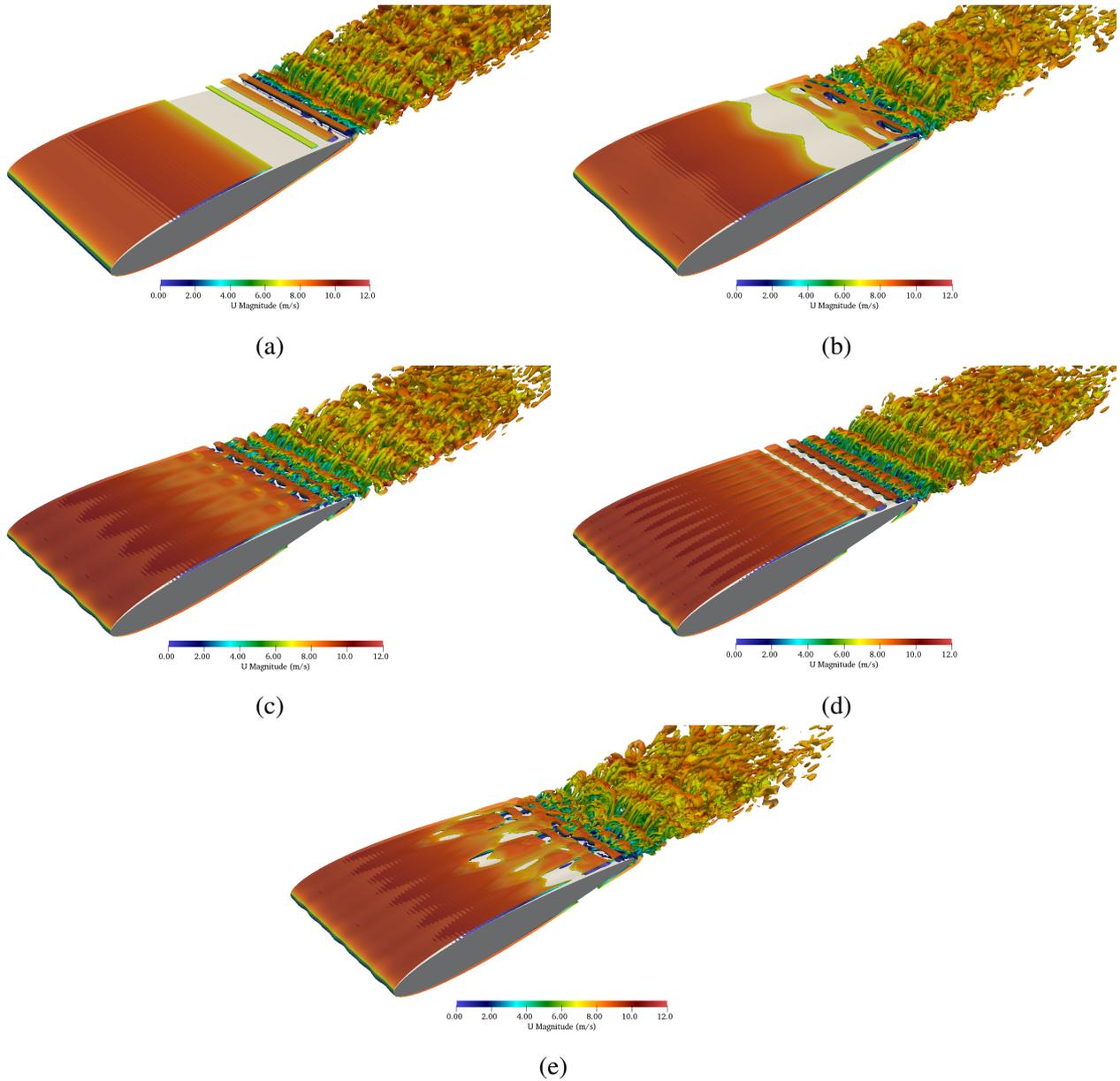
Figure 5: Iso-Q contours for (a) smooth wing, (b) variant 1, (c) variant 2, (d) variant 3, and (d) variant 4.

is strongly associated with tonal instability noise, and explains the results for the far-field noise. For the first three wavy wings, the vortices are altered by the presence of the surface waves, but the flow remains broadly two-dimensional. As one might expect, the surface waves do increase the fluctuation intensities in the boundary layer, with shorter surface waves increasing the intensity more than the longer waves. At $x/c = 0.9$, the span-averaged root-mean-square of the pressure coefficient is $C_p' = 0.053$ for the smooth foil, and this increases to $C_p' = 0.075,\ 0.102,\ 0.125$ for variants 1, 2, and 3 respectively. However, the wavy wings have significant spanwise variability in the fluctuations, with the intensity in the troughs being substantially lower than at the peaks and zero-crossing points. This reduces the scattering efficiency of the instability waves at the trailing edge, leading to an overall reduction in the sound levels. For variant 4, the pressure fluctuations drop to $C_p' = 0.069$ but it is the marked change in the spanwise correlation that leads to the sharp drop in the sound level. Whilst the instability waves remain in phase along the span for variants 1-3, this is not the case for variant 4.

The reason for the large difference in the sound pressure levels between variants 1-3 and variant 4
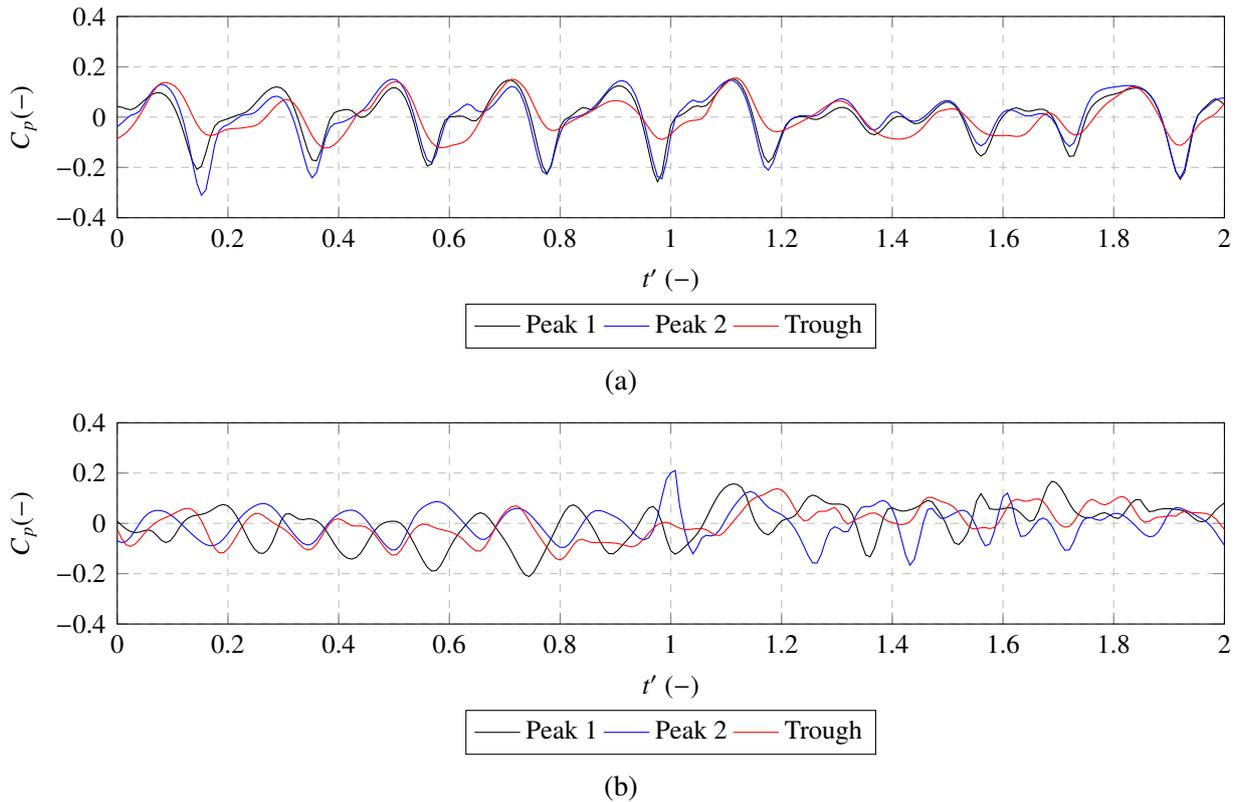
Figure 6: Flucutations in pressure coefficient over two chord-flow times for (a) variant 2, and (b) variant 4. Data are shown for three locations along the span at $x/c = 0.9$.

becomes clearer when considering the pressure fluctuations on the surface of the wings close to the trailing edge. Figure 6 shows time series of the pressure fluctuations at three spanwise locations for variants 2 and 4. These are shown at two consecutive peaks and the trough in between them. For variant 2, it is clear that despite differences in the amplitude of the fluctuations, they remain in-phase and the correlation between fluctuations at consecutive peaks is high. This contrasts markedly with variant 4, where the fluctuations for the two peaks are out of phase. This explains how the sound pressure level can be so much lower for this case.

Finally, it was stated in the introduction that the aim of the wavy wing is to reduce the sound level without increasing the drag. Table 1 shows the drag coefficient and the maximum overall sound pressure level for each case, together the drag coefficient determined using XFOIL [24]. This shows a small reduction in drag for variant 2, followed by a larger reduction for variants 3 and 4. Clearly, the best performing wing is variant 4, where a significant reduction in both the noise and drag is observed.

4. CONCLUSIONS

In this work, the results of a series of aeroacoustic simulations of wavy wings have been presented. A hybrid aeroacoustic model has been used, with large eddy simulations resolving the fluid field. Five wings have been considered: a NACA0012 wing and four variations with spanwise wavy surfaces. The first three variants have a spanwise sinusoidal variation whereas the surface of variant 4 has two sine waves superimposed to create a more random variation.

Due to the moderate Reynolds number and low angle of attack, the boundary layer on the suction side of the smooth NACA0012 wing is transitional, resulting in tonal trailing edge noise. For

Table 1: Maximum overall sound pressure level and drag coefficient for the five wings including a comparison with data from XFOIL [24].

Wing	Drag coefficient (-)	OASPL (dB)
XFOIL	0.022	-
Smooth	0.024	39.7
Variant 1	0.024	35.7
Variant 2	0.023	35.5
Variant 3	0.022	36.6
Variant 4	0.022	22.0

the variants with a single sinusoidal wave, a modest reduction of approximately 4 dB is achieved, alongside a small reduction in the drag for variants 2 and 3. For variant 4, a substantial drop in the noise levels is observed. This is attributed to a drastic reduction in the spanwise correlation of the instability waves in the boundary layer. As with variants 2 and 3, a modest decrease in drag is also observed for variant 4.

These results show that a wavy wing can be highly effective at reducing trailing edge instability noise and also reduce the drag. Further investigations are needed to understand the drag reduction mechanism and to develop a better understanding of how to optimise the surface geometry to minimise the noise.

ACKNOWLEDGEMENTS

REFERENCES

[1] H Arbey and J Bataille. Noise generated by airfoil profiles placed in a uniform laminar flow. *Journal of Fluid Mechanics*, 134:33–47, 1983.

[2] E C Nash, M V Lowson, and A McAlpine. Boundary-layer instability noise on aerofoils. *Journal of Fluid Mechanics*, 382:27–61, 1999.

[3] L E Jones and R D Sandberg. Numerical analysis of tonal airfoil self-noise and acoustic feedback-loops. *Journal of Sound and Vibration*, 330(25):6137–6152, 2011.

[4] T P Chong, P F Joseph, and M J Kingan. An investigation of airfoil tonal noise at different reynolds numbers and angles of attack. *Applied Acoustics*, 74(1):38–48, 2013.

[5] E Arcondoulis, C J Doolan, A C Zander, L A Brooks, and Y Liu. An investigation of airfoil dual acoustic feedback mechanisms at low-to-moderate reynolds number. *Journal of Sound and Vibration*, 460:114887, 2019.

[6] G Yakhina, M Roger, S Moreau, L Nguyen, and V Golubev. Experimental and analytical investigation of the tonal trailing-edge noise radiated by low reynolds number aerofoils. *Acoustics*, 2(2):293–329, 2020.

[7] T P Chong and P F Joseph. An experimental study of airfoil instability tonal noise with trailing edge serrations. *Journal of Sound and Vibration*, 332(24):6335–6358, 2013.

[8] L E Jones and R D Sandberg. Acoustic and hydrodynamic analysis of the flow around an aerofoil with trailing-edge serrations. *Journal of Fluid Mechanics*, 706:295–322, 2012.

[9] D J Moreau and C J Doolan. Noise-reduction mechanism of a flat-plate serrated trailing edge. *AIAA journal*, 51(10):2513–2522, 2013.

[10] F Avallone, WCP Van Der Velden, D Ragni, and D Casalino. Noise reduction mechanisms of sawtooth and combed-sawtooth trailing-edge serrations. *Journal of Fluid Mechanics*, 848:560–591, 2018.

[11] T Geyer, E Sarradj, and C Fritzsche. Measurement of the noise generation at the trailing edge of porous airfoils. *Experiments in Fluids*, 48(2):291–308, 2010.

[12] I A Clark, C A Daly, W Devenport, W N Alexander, N Peake, J W Jaworski, and S Glegg. Bio-inspired canopies for the reduction of roughness noise. *Journal of Sound and Vibration*, 385:33–54, 2016.

[13] V B Ananthan, P Bernicke, R A D Akkermans, T Hu, and P Liu. Effect of porous material on trailing edge sound sources of a lifting airfoil by zonal overset-les. *Journal of Sound and Vibration*, page 115386, 2020.

[14] J Wang, C Zhang, Z Wu, J Wharton, and L Ren. Numerical study on reduction of aerodynamic noise around an airfoil with biomimetic structures. *Journal of Sound and Vibration*, 394:46–58, 2017.

[15] K Volkmer, N Kaufmann, and T H Carolus. Mitigation of the aerodynamic noise of small axial wind turbines-methods and experimental validation. *Journal of Sound and Vibration*, 500:116027, 2021.

[16] J W Kim, S Haeri, and P F Joseph. On the reduction of aerofoil-turbulence interaction noise associated with wavy leading edges. *Journal of Fluid Mechanics*, 792:526–552, 2016.

[17] W Chen, W Qiao, F Tong, L Wang, and X Wang. Numerical investigation of wavy leading edges on rod–airfoil interaction noise. *AIAA Journal*, 56(7):2553–2567, 2018.

[18] B Dean and B Bhushan. Shark-skin surfaces for fluid-drag reduction in turbulent flow: a review. *Philosophical Transactions of the Royal Society A: Mathematical, Physical and Engineering Sciences*, 368(1929):4775–4806, 2010.

[19] T A Smith and Y Ventikos. A hybrid computational aeroacoustic model with application to turbulent flows over foil and bluff bodies. *Journal of Sound and Vibration*, page 116773, 2022.

[20] D J Moreau, L A Brooks, and C J Doolan. The effect of boundary layer type on trailing edge noise from sharp-edged flat plates at low-to-moderate reynolds number. *Journal of Sound and Vibration*, 331(17):3976–3988, 2012.

[21] W-W Kim and S Menon. A new dynamic one-equation subgrid-scale model for large eddy simulations. In *33rd Aerospace Sciences Meeting and Exhibit*, page 356, 1995.

[22] T A Smith and Y Ventikos. Boundary layer transition over a foil using direct numerical simulation and large eddy simulation. *Physics of Fluids*, 31(12):124102, 2019.

[23] T A Smith and Y Ventikos. Assessment of computational techniques for the prediction of acoustic sources from lifting surfaces using les and dns. In *Eighth International Conference on Computational Methods in Marine Engineering*, 2019.

[24] M Drela. Xfoil: An analysis and design system for low reynolds number airfoils. In *Low Reynolds number aerodynamics*, pages 1–12. Springer, 1989.